JGR Space Physics

RESEARCH ARTICLE
10.1029/2020JA028789

A Double Disturbed Lunar Plasma Wake

A. P. Rasca[1], S. Fatemi[2,3], W. M. Farrell[1], A. R. Poppe[4,5], and Y. Zheng[1]

[1]NASA Goddard Space Flight Center, Greenbelt, MD, USA, [2]Swedish Institute of Space Physics, Kiruna, Sweden, [3]Department of Physics, Umeå University, Umeå, Sweden, [4]Space Sciences Laboratory, University of California, Berkeley, CA, USA, [5]Solar System Exploration Research Virtual Institute, NASA Ames Research Center, Moffett Field, CA, USA

Key Points:

- Passing coronal mass ejection (CME) during a Full Moon distorts the magnetopause and magnetosheath, resulting in the Moon's removal from the geomagnetic tail
- CME arrival results in the redevelopment of a short optically misaligned lunar plasma wake
- Event conditions are favorable for the development of flux-rope like plasmoids in the magnetotail capable of being detected at the Moon

Correspondence to:
A. P. Rasca,
anthony.rasca@gmail.com

Citation:
Rasca, A. P, Fatemi, S., Farrell, W. M, Poppe, A. R, & Zheng, Y. (2021). A double disturbed lunar plasma wake. *Journal of Geophysical Research: Space Physics*, *126*, e2020JA028789. https://doi.org/10.1029/2020JA028789

Received 8 JUN 2020
Accepted 8 DEC 2020

Abstract Under nominal solar wind conditions, a tenuous wake forms downstream of the lunar nightside. However, the lunar plasma environment undergoes a transformation as the Moon passes through the Earth's magnetotail, with hot subsonic plasma causing the wake structure to disappear. We investigate the lunar wake response during a passing coronal mass ejection (CME) on March 8, 2012 while crossing the Earth's magnetotail using both a magnetohydrodynamic (MHD) model of the terrestrial magnetosphere and a three-dimensional hybrid plasma model of the lunar wake. The CME arrives at 1 AU around 10:30 UT and its impact is first detected inside the geomagnetic tail after 11:10 UT by the Acceleration, Reconnection, Turbulence and Electrodynamics of the Moon's Interaction with the Sun (THEMIS-ARTEMIS) satellites in lunar orbit. A global magnetospheric MHD simulation using Wind data for upstream conditions with the OpenGGCM model reveals the magnetosheath compression to the lunar position from 11:20–12:00 UT, accompanied by multiple flux rope or plasmoid-like features developing and propagating tailward. MHD results support plasma changes observed by the THEMIS-ARTEMIS satellites. Lunar-scale simulations using the Amitis hybrid code show a short and misaligned plasma wake during the Moon's brief entry into the magnetosheath at 11:20 UT, with plasma expansion into the void being aided by the higher plasma temperatures. Sharply accelerated flow speed and a compressed magnetic field lead to an enhanced electric field in the lunar wake capable of generating sudden changes to the nightside near-surface electric potential.

1. Introduction

The lunar environment is directly exposed to space plasma in the solar wind or while in the geomagnetic tail. While the lunar plasma environment in the solar wind and the geomagnetic tail are often modeled separately, there are occasions when the two are spatially linked. For example, the geomagnetic tail can become highly dynamic and deformed during the passing of a coronal mass ejection (CME), which applies pressure directly to the magnetotail of the Earth. In this work, we examine the near-Moon plasma environment during a time at which the lunar plasma environment is disturbed by both the geomagnetic tail and effects from a passing CME (effectively, "double disturbed").

For approximately three quarters of its orbit, the Moon is exposed to the solar wind environment outside the Earth's magnetotail. The solar wind plasma is mainly composed of protons and electrons flowing radially out from the Sun with a typical speed at 1 AU of ~400 km/s, ion density of ~5 cm^{-3}, and ion/electron temperatures of ~10 eV. The near-surface lunar environment is heavily influenced by the solar wind plasma flow and intense radiation from the Sun as the dayside surface charges a few volts positive due to radiation-driven photoemission (Manka, 1973; Poppe & Horányi, 2010). Loss of these solar wind particles on the dayside creates a downstream plasma void, where the nightside surface is impacted predominantly by solar wind electrons, charging the surface negatively (Farrell et al., 2010; Halekas et al., 2009, 2008; Nishino et al., 2017; Rhodes & Farrell, 2019). Refilling the downstream plasma wake generates a complex nightside charging environment due to the development of an ambipolar electric field at the wake flank that acts to divert solar wind ions into the wake (Crow et al., 1975; Fatemi et al., 2012; Rhodes & Farrell, 2019; Xu et al., 2019; Zimmerman et al., 2011). On the global scale of the Moon, this effect has been observed by Explorer 35, Lunar Prospector (LP), Acceleration, Reconnection, Turbulence and Electrodynamics of the Moon's Interaction with the Sun (THEMIS-ARTEMIS), Kaguya, and Chandrayaan-1 spacecraft during transits through the lunar wake (Colburn et al., 1967; Dhanya et al., 2016; Halekas et al., 2011, 2005; Nishino et al., 2009; Xu et al., 2019; Zhang et al., 2014). There have also been numerous modeling studies focusing

on the lunar wake structure under nominal solar wind conditions using magnetohydrodynamic (MHD) descriptions (e.g., Cui & Lei, 2008; Spreiter et al., 1970; Xie et al., 2013) as well as particle (e.g., Birch & Chapman, 2001; Farrell et al., 1998) and hybrid models (e.g., Fatemi et al., 2012, 2013; Holmström et al., 2012; Poppe et al., 2014; Wang et al., 2011). Moreover, the refilling process is affected by extreme events such as solar storms that alter the interplanetary magnetic field (IMF) and plasma properties/composition of the solar wind. In the case of a halo (Earth-directed) CME, the solar wind is replaced with hot dense plasma released from the solar corona and accelerated to velocities exceeding 600 km/s (Richardson & Cane, 2010).

The lunar plasma environment undergoes another transformation as the Moon spends the other quarter of its orbit traversing the Earth's downstream magnetosphere. Upon crossing the transitional magnetosheath region, the Moon enters the hot and relatively tenuous magnetotail. In the magnetotail the plasma ion density is reduced to $n < 0.5$ cm^{-3} and the flow slows to less than 100 km/s (Lui, 1987; Troshichev et al., 1999). While transiting the magnetotail, the Moon can pass through or very near the plasma sheet, a region dividing the north and south lobes and characterized by hotter and more dense plasma relative to the rest of the magnetotail (Sibeck & Lin, 2014). In the plasma sheet, a $-u_x$-dominated plasma velocity is expected, where $+x$ points in the sunward direction. Due to the, overall low density and velocity in the magnetotail relative to the ambient solar wind, the plasma flow in the magnetotail region is effectively "turned off". The reduced plasma flow can result in a severely altered and diminished lunar wake, as demonstrated in hybrid simulations by Vernisse et al. (2013), or possibly a sunward wake observed by THEMIS-ARTEMIS (Ma et al., 2015).

Numerous studies—both observational and theoretical—have already shown a complex and dynamic lunar surface plasma environment within the Earth's magnetotail. For example, Halekas et al. (2008) used data from the LP spacecraft to compare the nightside lunar electrostatic surface potential in the magnetotail with the nightside surface in the ambient solar wind, showing surface potentials of ∼−100 V as the Moon passes through the magnetotail lobes that can drop to −1 kV while crossing the plasma sheet. LP observations and one-dimensional particle-in-cell (PIC) simulations also show that large negative potentials can develop on the lunar dayside while in the terrestrial plasma sheet (A. Poppe et al., 2011). However, in the highly tenuous magnetotail lobes, the lunar surface potential increases to around +40–200 V due to photoemission dominating completely over ambient electron collection (Harada et al., 2013, 2017).

Although the Moon spends nearly a quarter of its time in the terrestrial magnetotail, only a small number of theoretical studies have addressed the lunar plasma environment within the Earth's magnetotail. Vernisse et al. (2013) used a hybrid code to gradually reduce the plasma flow speed (holding the plasma density n constant) around a lunar-type obstacle to below the Alfvénic speed, u_a. For nominal solar wind conditions ($|u| = 8u_a$, $n = 5$ cm^{-3}), a plasma void of $n < 0.5$ cm^{-3} extends several lunar radii downstream of the nightside. As they reduce the flow to sub-Alfvénic speeds typical of the geomagnetic tail ($\sim 0.5u_a$), the wake structure with $n < 0.5$ cm^{-3} vanishes. Harnett and Winglee (2013) showed the lunar wake response to a magnetic flux rope in the slow tenuous plasma of the magnetotail using a MHD model to reveal misaligned lunar plasma and optical wakes. While MHD models are ideal for modeling space weather events on the scale of planetary magnetospheres, they do not fully capture kinetic processes associated with ion populations shown to influence wake refilling at lunar scales (Fatemi et al., 2012, 2014; Holmström et al., 2012).

In this study, we consider the case of an Earth-directed CME and the terrestrial magnetotail environment disturbing the lunar wake simultaneously. This occurred on March 8, 2012 as a halo CME reached the Earth at 1 AU around 10:30 UT (Patsourakos et al., 2016) during a nearly full Moon, when the Moon would nominally be in the central geomagnetic tail. We use spacecraft data as upstream boundary conditions for a set of numerical simulations to first model the response of the Earth's global magnetosphere (GM) using a MHD model. A second small-scale set of simulations using a hybrid code (see Section 3) focuses on the response of the lunar wake when the magnetotail is first disturbed by the CME shock and plasma sheath. Shang et al. (2020) reported independently on the effect of the disturbed geomagnetic tail at the Moon itself using THEMIS-ARTEMIS observations. As we discuss below, we reach very similar conclusions regarding the nature of the fast flows observed during the full Moon period. We have herein also examined how these anomalous fast flows affected the formation of the trailing lunar wake.

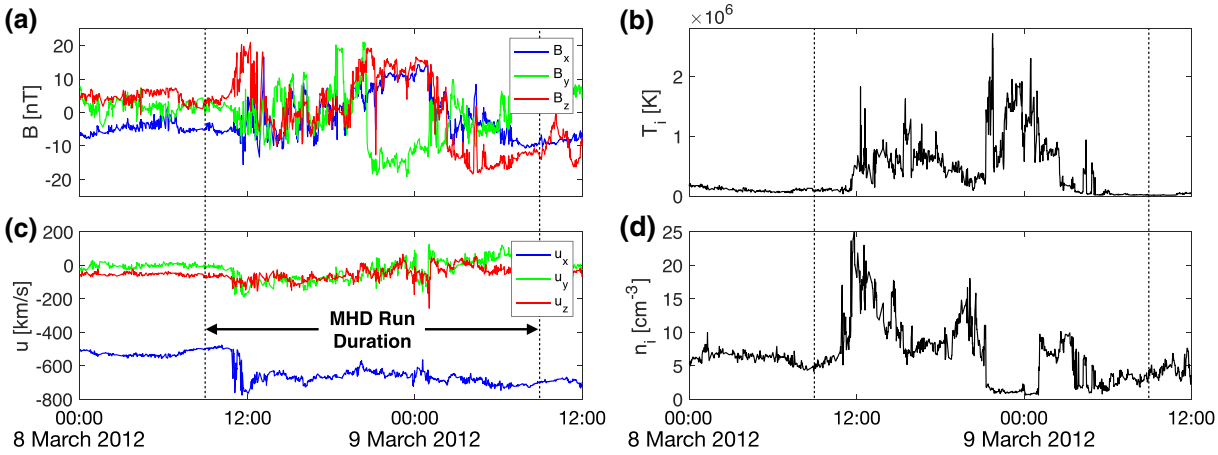

Figure 1. Plasma parameters during the coronal mass ejection (CME) passage on March 8 and 9, 2012 as observed by the Wind spacecraft upstream of the Earth's bow shock\enleadertwodots Displayed are (a) the magnetic field, (b) ion temperature, (c) plasma velocity, and (d) ion density. The vertical lines indicate the start and end times for the time-dependent magnetohydrodynamic (MHD) model of the global magnetosphere (GM).

In this paper, we begin by describing the observed CME event in the following section. A thorough description of the MHD model run through the Community Coordinated Modeling Center (CCMC) located at NASA Goddard Space Flight Center will be made in Section 3, followed by MHD results showing the initial response of the GM to the CME. In Section 4 we will describe the hybrid code used for modeling the lunar wake, along with advantages of our selections of models for the large-scale (MHD) and small-scale (hybrid) simulations. We will present hybrid results in Section 5 using both nominal solar wind upwind conditions and plasma parameters extracted from THEMIS-ARTEMIS data in the magnetotail during the CME. We conclude with analysis and conclusions of our results.

2. CME Observations

We selected a CME event to use in our simulations based on three criteria: (1) the event is a halo (Earth-directed) CME, (2) the CME shock arrives at 1 AU at most 12 h prior to or following a full Moon, and (3) the CME is well-observed (in situ) both outside and inside the Earth's magnetotail. Criteria (1) and (3) are self-evident, but (2) was chosen to ensure the Moon lies within typical magnetotail boundaries during the CME-induced geomagnetic storm (the Moon on average takes 4 days to cross the magnetotail). A search of observed CME events from 2011 to 2018 yielded only one that fit all three criteria: a halo CME associated with an X-class flare originating from active region NOAA 11429 on March 7, 2012 arrived at 1 AU around 10:30 UT on March 8, 2012 (Patsourakos et al., 2016), less than 3 h before a full Moon. The CME was observed by the Wind spacecraft in the solar wind at the L_1 Lagrangian point and the magnetospheric response was detected by the pair of THEMIS-ARTEMIS satellites (P1 and P2) in lunar orbit. This event—from the Sun to Earth—is also well-studied in multiple articles (Liu et al., 2013; Patsourakos et al., 2016; Shang et al., 2020).

Solar wind and CME plasma measurements by the Wind spacecraft are plotted in Figure 1. Patsourakos et al. (2016) shows the solar wind already perturbed by CME events the previous day (not shown here), but it returns to near-nominal conditions during the hours preceding the plasma shock, with a plasma velocity ~500 km/s, $|B| \approx 7$ nT, $n_i \approx 5$ cm^{-3}, and $T_i \approx 9$ eV. The plasma shock at 10:30 UT is indicated by sharp near-discontinuous jumps in the magnitudes of each plasma parameter in Figure 1. This is followed by the plasma sheath that is characterized by an accelerated hot and dense plasma flow. The structure changes again around 18:00 UT as the interplanetary CME (ICME) begins to pass. Despite the multi-day duration of the entire CME and geomagnetic storm, we will be most concerned with investigating the disturbed magnetosphere and magnetotail during the plasma shock and sheath since the plasma environment undergoes the most drastic changes during this time.

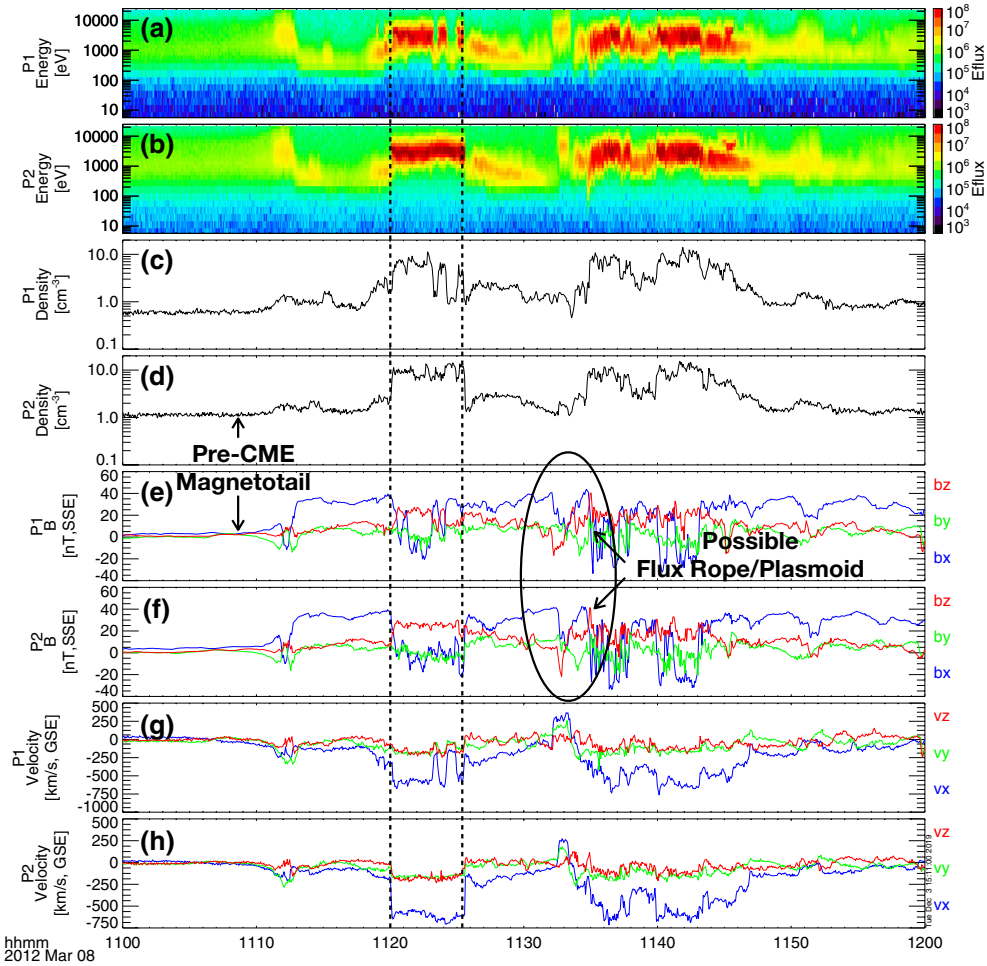

Figure 2. THEMIS-ARTEMIS P1 and P2 plasma data in the vicinity of the Moon during the CME shock and plasma sheath arrival. Displayed are (a–b) the ion energy flux, (c–d) ion density, (e–f) magnetic field, and (g–h) plasma velocity for each THEMIS-ARTEMIS probe, respectively. Upstream plasma conditions for the Amitis run are extracted from the average plasma parameters between the vertical dashed lines. coronal mass ejection, CME, Acceleration, Reconnection; THEMIS-ARTEMIS, Turbulence and Electrodynamics of the Moon's Interaction with the Sun.

The CME-induced disturbance in the terrestrial magnetotail was detected by THEMIS-ARTEMIS around 11:10 UT, only 40 min after the plasma shock by the Wind spacecraft. The two THEMIS-ARTEMIS satellites (P1 and P2) were originally part of the THEMIS mission composed of five identical spacecraft studying the Earth's magnetosphere in high-Earth orbit. P1 and P2 were later positioned for lunar orbit in June 2011 and July 2011, respectively, to study the magnetotail, solar wind, and lunar environment (Angelopoulos, 2010). Both spacecraft are equipped with several instruments for observing the magnetosphere environment, including a set of magnetometers and electrostatic analyzers (Auster et al., 2008; McFadden et al., 2008; Roux et al., 2008), providing plasma measurements that are the primary focus of this study. We also place particular focus on THEMIS-ARTEMIS data obtained during the initial plasma shock and plasma sheath arrival. This is not only due to the dramatic transformation of the plasma environment in the magnetotail, but also due to the remainder of the event taking place during periods of low telemetry rates from the THEMIS-ARTEMIS satellites.

Figure 2 shows plasma measurements from both THEMIS-ARTEMIS P1 and P2 during the initial magnetotail disturbance by the CME shock and plasma sheath. During this time, P1 and P2 are located downstream from the Moon and outside its optical wake at $[-10, 3.7, -1.7]$ R_M and $[-8.6, 4.5, 1.1]$ R_M, respectively, in SSE coordinates. Prior to 11:10 UT, typical magnetotail conditions are observed, with a very slow and

low-density ambient plasma flow and $B_x > 0$ indicating the probes are located in the northern magnetotail lobe. Starting shortly after 11:10 UT, a B_x-dominated magnetic field disturbance penetrates to the inner magnetotail, followed by further magnetic field structural changes and a hot dense plasma now engulfing the Moon. From 11:20 to 11:25 UT, the Moon is immersed in a supersonic plasma flow, changing abruptly at 11:20 UT from near-stationary to over 700 km/s. The period of intense flow abruptly ends at 11:25 UT. During this time, the plasma density at both THEMIS-ARTEMIS satellites jumps from around 1 cm^{-3} to nearly 10 cm^{-3}. Following these brief coherent structures, there exists a much more dynamic plasma from 11:32–11:48 UT, with an interesting magnetic field signature at the beginning of this timeframe. Beginning at 11:32 UT both spacecraft observe changes in the magnetic field structure that resemble magnetic field signatures for flux rope-like plasmoids seen by Jackman et al. (2014) in other planetary magnetotails. The negative-to-positive reversal in B_z during a gradual increase and decrease in $\mathrm{mag}\left(\left[B_x, B_y\right]\right)$ matches what was seen when Jackman et al. (2014) demonstrated a spacecraft passing through a flux rope-like plasmoid, characterized as a helical magnetic structure moving downstream in a planetary magnetotail. This signature in the data also corresponds with a brief reversal of the plasma flow in the x-direction, which has been observed by THEMIS-ARTEMIS in connection with passing flux ropes in the terrestrial magnetotail in a study by Kiehas et al. (2012). Their results show B_z initially positive and becoming negative, opposite of the reversal seen at 11:33 UT in Figure 2, indicating the magnetic feature is traveling in either a tailward direction north of the probes or Earthward south of the probes. The potential plasmoid or flux rope is followed by another fast dense plasma stream, before a period of tenuous conditions similar to the undisturbed magnetotail.

We see a wide variety of dynamic plasma features described above. Due to, limitations that will be addressed in a later section, small-scale hybrid simulations of the lunar wake were run using average plasma parameters extracted during 11:20–11:25 UT (indicated by the dashed vertical lines) as upstream conditions. However, the large-scale MHD simulation of the GM during the CME event aims to contextualize several features described from 11:10–11:50 UT.

3. Global Magnetosphere Response

3.1. Magnetohydrodynamic Model

To model the terrestrial magnetospheric response to the CME, we use a MHD code available at the CCMC. While fully kinetic PIC or hybrid-PIC plasma codes are available, they are most useful for length scales smaller or comparable to the gyro-radii of ions (≈100 km for solar wind protons). Models for large-scale storm structures propagating through the inner heliosphere (IH) and for GMs operate on length scales (multiple planetary radii) large enough for small-scale particle dynamics to be ignored. More on the appropriate scales for hybrid models will be discussed in a later section.

For our simulation run through the CCMC, we use the Open Geospace General Circulation Model (OpenGGCM) developed by Raeder et al. (2008). OpenGGCM is an MHD model designed for the coupled terrestrial magnetosphere, ionosphere, and thermosphere on a three-dimensional computational domain measuring $[x_{\min}, x_{\max}] \times [y_{\min}, y_{\max}] \times [z_{\min}, z_{\max}] = [-350, 33] \times [-96, 96] \times [-96, 96]\ R_E$, where $R_E = 6,371$ km is the radius of the Earth. Our MHD simulation uses Wind data from Figure 1 as time-dependent upwind boundary conditions for a 24-h run starting at 9:00 UT on March 9, 2012, 90 min before the CME shock arrival at 1 AU. The simulation interval is represented by the two vertical dashed lines in Figure 1, though only the first few hours during the shock and plasma sheath arrival are analyzed and compared in this study.

3.2. Magnetosphere Configuration During the CME Passage

Figures 3 and 4 show slices of the plasma density and flow speed for $y = 0\ R_E$ (left columns) and $z = -5\ R_E$ (right columns), where Earth is at the origin, $+x$ points from the Earth to the Sun and z is perpendicular to the ecliptic plane. Figure 5 shows the plasma temperature for $y = 0$ at the 10:00 UT (pre-shock) and 11:33 UT (post-shock). The Moon is located downstream in the magnetotail at $(x, y, z) \approx (-60, 0, -5)R_E$. At four different times during the OpenGGCM run, the figures show the plasma density (with the magnetic field

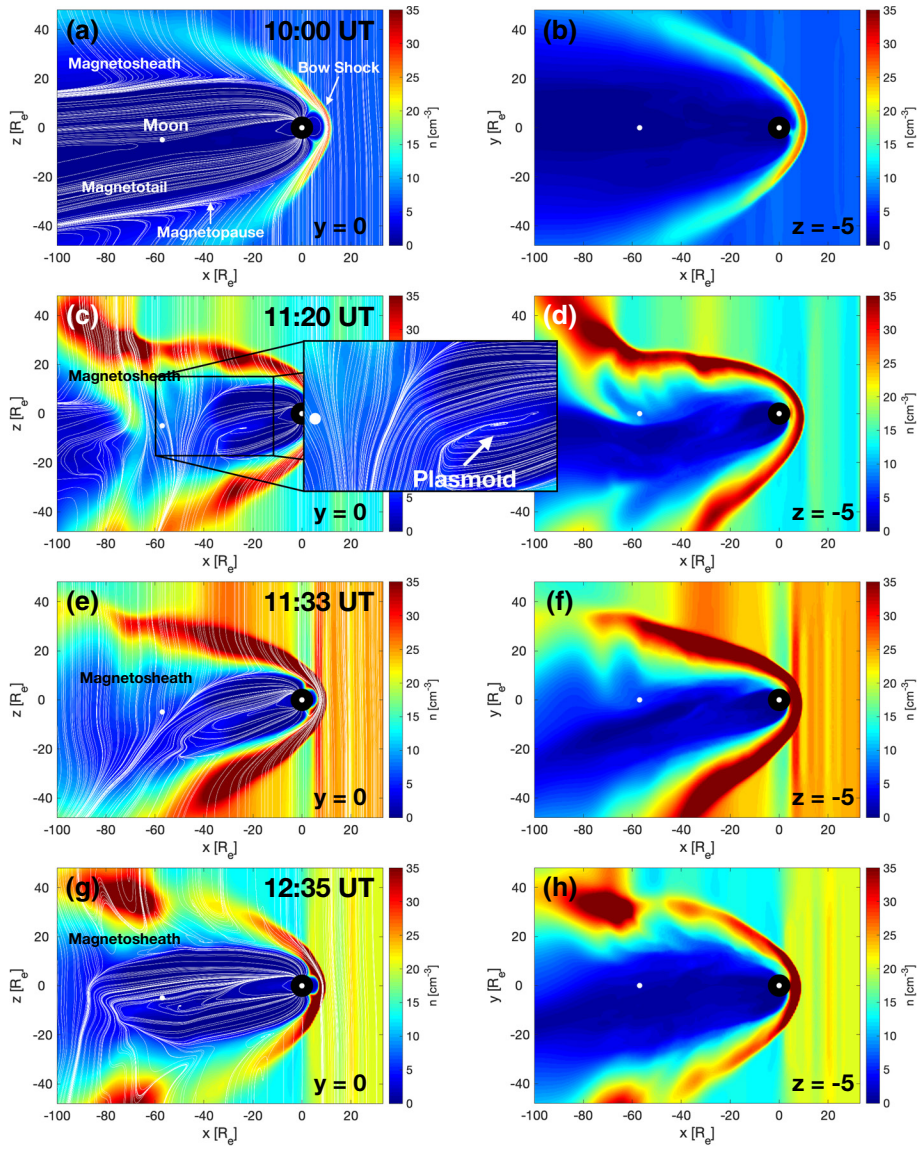

Figure 3. Magnetohydrodynamic (MHD) results of the plasma density for y = 0 (left column) and z =−5 RE (right column), both containing the Moon at 10:00 UT (a–b; pre-shock), 11:20 UT (c–d), 11:33 UT (e–f), and 12:35 UT (g–h) on March 8, 2012. The white disk to the right of the Moon represents the Earth. Magnetic field lines in the xy-plane overlay the y = 0 density contour plots. The shifting location of the magnetosheath is indicated at each time.

overlaid for $y = 0$) and the plasma velocity. The first row of each figure shows the terrestrial magnetosphere at 10:00 UT on March 8, 2012, shortly before the CME shock enters the computational domain. The second and third rows show the magnetotail as it is initially distorted by the plasma shock and the plasma sheath, respectively. The last row shows a time after which the Moon returned to the central magnetotail.

Initially, the Moon is located in the tenuous and nearly stationary magnetotail plasma in the northern lobe just above the hot plasma sheet. The fast-flowing plasma sheet is evident in Figure 5, appearing as a thin line extending down the middle of the magnetotail in the *xz*-plane. As the CME arrives at 1 AU, the magnetopause boundary distorts inward toward the magnetotail, causing the Moon to enter the warm inner flanks of the magnetosheath (11:20 UT and 11:33 UT). During this period, under the pressure of the CME, the magnetotail develops a strong negative *yz*-component shift in position from the nominal − *x*-direction (Figures compare 4b and 4d), possibly due to a slight oblique velocity angle following the shock. Note from Figure 1c that the post-shock plasma has a v_y flow in excess of 150 km/s. In doing so, the Moon becomes

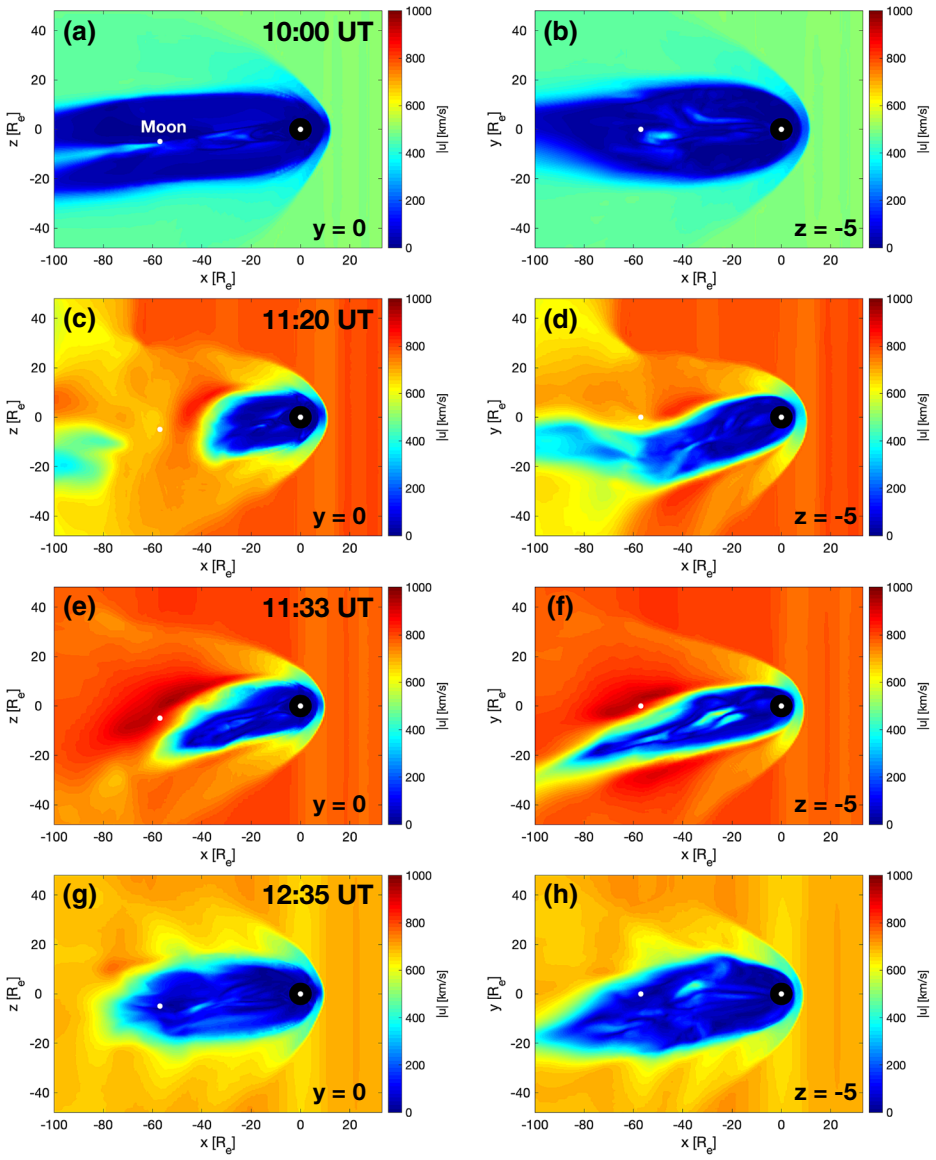

Figure 4. Magnetohydrodynamic (MHD) results of the plasma velocity corresponding to the same times and two-dimensional slices as Figure 3.

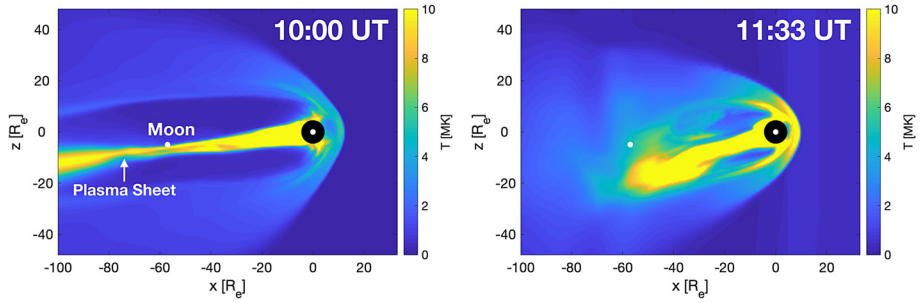

Figure 5. Plasma temperature in the *xz*-plane from the Magnetohydrodynamic (MHD) results showing pre-shock (left) and post-shock (right) temperature conditions. The plasma sheet is indicated in the pre-shock panel.

Table 1
Upstream Plasma Parameters for Hybrid Simulations

	Nominal solar wind	Disturbed magnetotail plasma
n_i (cm^{-3})	5	11
T_i (K)	1×10^5	1.7×10^6
u (km/s)	[−400, 0, 0]	[−670, 200, 0]
B (nT)	[−4.9, 4.9, 0]	[−5, 0, 25]

engulfed in the fast-flowing magnetosheath plasma (Figures 4c–4f). Also during this time interval in the simulation, a magnetic feature resembling a plasmoid is observed developing and drifting downstream in the magnetosphere (Figure 3c inset). Due to the stochastic nature of plasmoid formation, we do not expect a one-to-one correspondence of simulation plasmoids/flux ropes and THEMIS-ARTEMIS-observed plasmoids/flux ropes. However, the MHD simulation does inform us that the conditions were ripe for plasmoid formation during the passage of the CME. Approximately an hour later, the flow speed and density outside the magnetosphere begin to decrease (Figures 1c–1d) and lunar exposure to the magnetosheath decreases as the magnetotail re-establishes a more typical configuration (Figures compare 4f and 4h). The CME will continue distorting the magnetosphere for several hours.

The MHD results support patterns observed by the THEMIS-ARTEMIS satellites in Figure 2. Magnitude changes in the plasma velocity and temperature detected by THEMIS-ARTEMIS indicate that the Moon is no longer in the magnetotail during those times, but rather in the magnetosheath or possibly in the CME proper. Note in Figures 2a and 2b, that the ions are now a quasi-monoenergetic and anti-sunward flow like that in the magnetosheath or solar wind. Also, in Figures 2c and 2d, the plasma density increases by over a factor of 10 to ∼10 cm^{-3}, suggesting again that the THEMIS-ARTEMIS satellites are in the magnetosheath. Figures 3 and 4 reveal that the sudden change in plasma conditions are likely due to the distorted and compressed magnetosphere, causing the Moon to fully exit the magnetotail and enter into the magnetosheath. Furthermore, the noted plasmoid propagating toward the Moon in our MHD run supports our interpretations of the magnetic field profiles around 11:32 UT in the THEMIS-ARTEMIS data. Possible lunar crossings into the magnetosheath in connection with an oblique shock arrival agree with similar MHD simulations performed by Shang et al. (2020). Their simulation incorporated the oblique shock front into the upstream boundary conditions and demonstrated a more brief "flapping" cycle of the magnetotail (∼340 s) that more appropriately matches the timescale of the probes' departure and re-entry into the magnetotail from 11:20–11:25 UT.

4. The Anomalous Appearance of a Lunar Wake at Full Moon

4.1. Hybrid Model and Setup

Lunar wake models are run using the Amitis code (Fatemi et al., 2017). Amitis is a GPU-based, three-dimensional hybrid model that describes the plasma interaction of planetary bodies with ambient plasmas and differs from a purely fluid model by treating the electrons as a massless fluid and ions as particles. This model is ideal to study the solar wind plasma interaction with the Moon as the solar wind ion gyro-radius is smaller or comparable to the size of the Moon. This allows the hybrid model to provide a more accurate description of the ion physics at this scale while not being as computationally expensive as a purely kinetic model. Numerous studies have used Amitis to model solar wind interactions with planetary bodies ranging in size from asteroids to Mercury (Fatemi et al., 2017, 2018, 2020 Fatemi & Poppe, 2018; Fuqua Haviland et al., 2019; Garrick-Bethell et al., 2019; Poppe, 2019).

Amitis runs were performed assuming a lunar conductivity of 10^{-7} S/m and using two different sets of time-dependent upstream boundary conditions, each running until a steady-state is obtained. The first run assumes nominal solar wind plasma conditions on a computational domain measuring $[x_{min}, x_{max}] \times [y_{min}, y_{max}] \times [z_{min}, z_{max}] = [-7, 2] \times [-3.7, 3.7 \times [-3.7, 3.7]\ R_M$, where R_M = 1,737 km is a lunar radius and the coordinate axes are oriented similarly to the MHD simulations with the $+x$ axis pointing toward the Sun, but with the Moon at the origin in the hybrid simulation box. The second run uses the magnetotail plasma conditions extracted from THEMIS-ARTEMIS data between 11:20 and 11:25 UT in Figure 2 on a domain measuring $[x_{min}, x_{max}] \times [y_{min}, y_{max}] \times [z_{min}, z_{max}] = [-5.7, 4.6] \times [-4.6, 8] \times [-4.6, 4.6]\ R_M$ to account for the $+y$-component of the plasma velocity. As revealed by the MHD results in the previous section, these parameters likely represent the Moon's brief entry into the magnetosheath, but will be referred to as disturbed magnetotail plasma. Plasma parameters for each run are shown in Table 1. To extract the disturbed

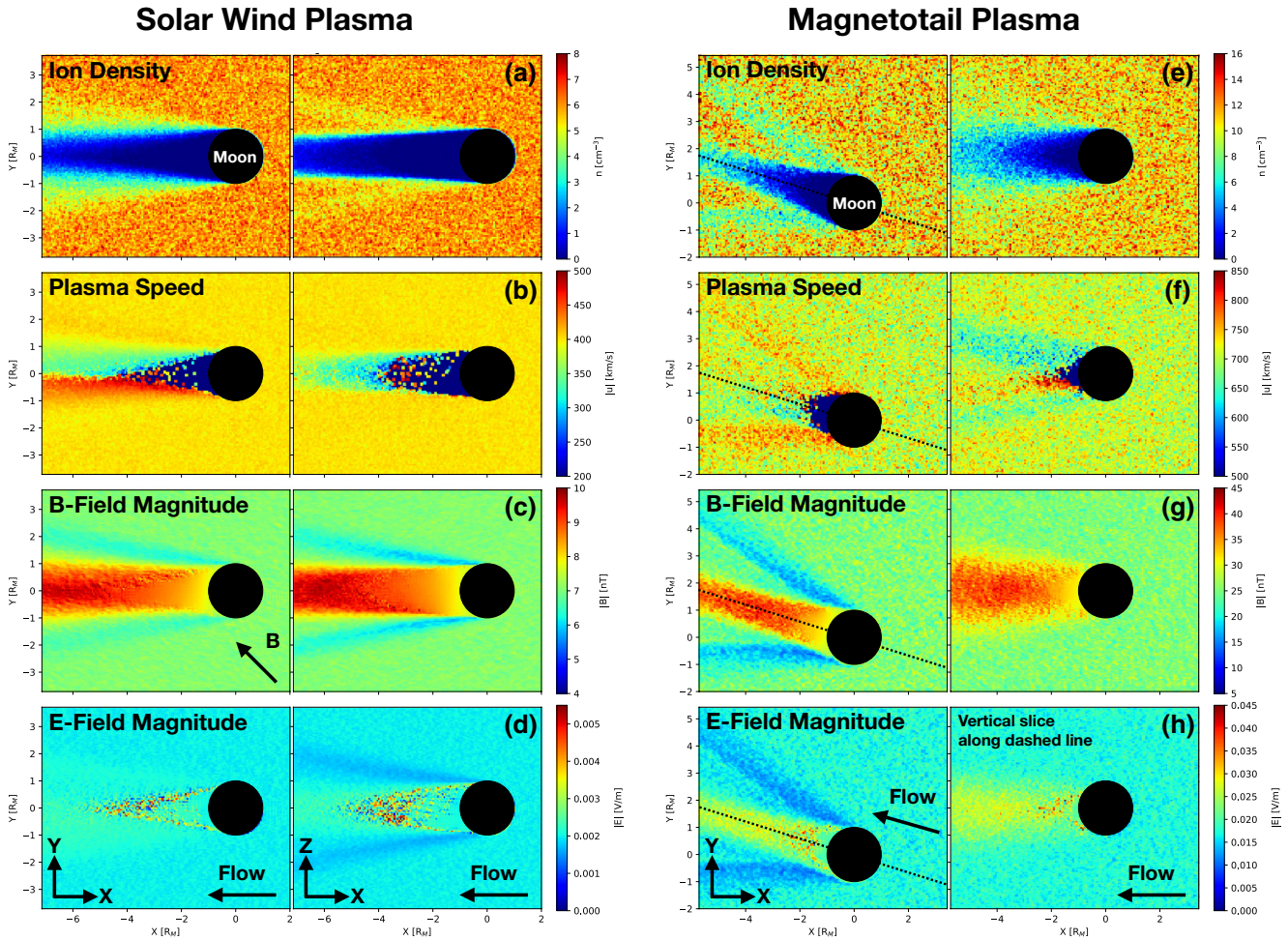

Figure 6. Amitis results using nominal solar wind conditions (left) and disturbed magnetotail conditions (right). Result for (top to bottom) the ion density, plasma speed, electric field, and magnetic field strengths are shown in both the *xy*- and *xz*-planes. The vertical plane (right-most column) for magnetotail conditions is taken along the dashed line in the *xy*-plane.

magnetotail plasma parameters in Table 1, a subtraction was necessary due to background penetrating radiation affecting parameters in Figure 2. Nominal solar wind parameters reflect pre-CME conditions at 1 AU outside the Earth's magnetosphere and assumes a 45° Parker spiral for the local IMF. The plasma parameters are selected to show how conditions initially and suddenly change immediately following CME arrival. Using THEMIS-ARTEMIS observations from 11:30 onward will be explored in future studies.

5. Results

Amitis results for the lunar wake during nominal solar wind conditions are shown in Figures 6a–6d as cuts in the *xy*- and *xz*-planes. A clear elongated void with a compressed magnetic field forms on the nightside, similar to hybrid results by Holmström et al. (2012) when using a 45° Parker spiral for the IMF. A rarefaction cone is evident in the *xz*-plane of panel (a), characterized by lower ion density originating from the north and south terminators, while in the *xy*-plane ions are more effectively diverted into the wake.

Under normal circumstances, the magnetotail plasma has a low flow speed and a high thermal speed, resulting in a diminished lunar wake at full Moon (Poppe et al., 2014). However, due to the large lateral distortion of the geomagnetic tail during the passing CME, the Moon finds itself in a fast supersonic plasma flow even when directly downstream from the Earth where the Moon would typically be in the central

magnetotail. Figures 6e–6h shows the wake structure when using the disturbed magnetotail conditions. The tleft panels show slices in the *xy*-plane. However, since the plasma flow is deflected from the *x*-axis in the *xy*-plane, vertical slices are taken along the flow direction, indicated by the dashed line in the left panels. A major difference from using solar wind conditions is a deflected flow in the + *y*-direction. The increased velocity and density do not only differ from the nominal solar wind, but also from typical magnetotail conditions in Table 1.

A much shorter wake forms on the lunar nightside in Figures 6e–6h, with low ion densities of <1 cm^{-3} extending only 1 R_M downstream from the nightside surface and ions filling in quickest in the vertical direction. We note that the wake appears to be smaller in size relative to wake formation in the nominal solar wind (Holmström et al., 2012). However, this effect is likely due to the higher magnetosheath plasma temperature that enhances the plasma expansion process. From the disturbed magnetotail plasma parameters (Table 1) near 11:20 UT in Figure 2, we find that the Moon is in a warm plasma—much warmer than in the solar wind and magnetotail (with the exception of the plasma sheet). The wake scale-size is a function of the ratio of u_{SW}/c_s (Farrell et al., 2002; Halekas et al., 2014), where c_s is the ion sound speed. For warm electrons, this ratio decreases compared to nominal solar wind conditions, giving rise to relatively quicker expansion into the wake and smaller extension of the downstream wake structure.

Several similarities between the nominal and double-disturbed wakes in Figure 6 still exist. While the flow in the disturbed magnetotail is misaligned from a purely − *x*-direction, it remains in the horizontal plane. However, the magnetic field is now *z*-dominated and nearly perpendicular to the wake normal in the *xy*-plane. The result is a prominent rarefaction and recompression region forming (a fluid process) along that wake boundary, which has also been observed by Holmström et al. (2012) while using a similar flow and magnetic field orientation, but for the solar wind.

One substantial aspect of the double disturbed wake is the enhanced electric field within the wake. The electric field in the wake (Figure 6h) is approximately 0.03–0.035 V/m, nearly a factor of 7 greater than in the solar wind wake (Figure 6d) with electric fields closer to 0.005 V/m. Note that the background electric field in the warmer double-disturbed plasma is close to 0.015 V/m, likely due to a faster flow speed and stronger magnetic field than in the solar wind. Also, flow velocity and the magnetic field are further increased in magnitude and remain nearly orthogonal in the central wake in Figure 6h, leading to a larger | u× B|.

6. Conclusions

We examined a unique pairing of events for the lunar wake environment during a lunar crossing of the terrestrial magnetotail that coincided with an Earth-directed CME passage on March 8, 2012. The GM response to the CME was studied using measurements from the Wind spacecraft while THEMIS-ARTEMIS observations provided context at the Moon during the initial shock and plasma sheath. The THEMIS-ARTEMIS observations were in turn used as upstream boundary conditions for a hybrid simulation of the lunar wake during the initial impact from the CME event and the results were compared with hybrid simulation output for the lunar wake under nominal solar wind conditions.

The MHD results help explain and provide context to other important plasma changes in the THEMIS-ARTEMIS observations. As the CME arrives at 1 AU, distortions of the magnetopause and magnetosheath cause the Moon to be removed from the magnetotail and become completely engulfed by the magnetosheath, before returning to the magnetotail less than an hour later. The $z = -5\ R_M$ slices in Figure 3 show the Moon's removal from the magnetotail is not due to the tail vanishing, but rather due to the entire magnetotail shifting in the −*y*- and −*z*-direction.

A notable result from modeling the GM response is the demonstration that conditions were favorable for generating several flux-rope like plasmoids, similar to that passing near the Moon around 11:32 UT and the flux rope studied by Harnett and Winglee (2013) at lunar scales. The magnetic field signature indicated in Figure 3 occurred during an extended period in the MHD simulations that has multiple plasmoid-like structures developing and propagating down the magnetotail. This implies magnetic structures in the

magnetotail—such as plasmoids or flux ropes—propagating to or very near the Moon could be common during passing CMEs, which sharply alter the surrounding magnetic field during a short period of time.

Using the hybrid model to simulate the plasma around the Moon from 11:20 to 11:25 UT reveals a shortened misaligned wake compared to the lunar wake during nominal solar wind conditions. While, the flow speed exceeds solar wind conditions, the higher plasma temperature helps accelerate expansion into the nightside void, resulting in the shorter wake. The MHD simulation aids our understanding of the hybrid results by suggesting we are effectively modeling the lunar wake in magnetosheath plasma. Follow-up theoretical studies will focus on a more in-depth study of hybrid simulations using time-varying upstream parameters for the magnetic field to mimic the plasmoid-associated changes indicated in Figure 2.

While the Earth's magnetosphere is often regarded as a protective shield against space weather effects, this study demonstrates that the lunar surface and surrounding plasma environment are susceptible to the impacts of a CME while inside the magnetotail. As we show, during the passage of the March 8, 2012 CME, the geomagnetic tail quickly swings in the $-y$- and $-z$-direction and a lunar wake forms having a substantially stronger electric field than during nominal solar wind conditions by a factor of 7. A related near-surface potential change is expected to be felt by any human systems on the lunar nightside. Future studies are needed to fully understand the effect these very abrupt changes in the lunar wake will have on the nightside surface charging environment.

Data Availability Statement

All THEMIS-ARTEMIS and Wind data necessary for this study are publicly available online (https://cdaweb.gsfc.nasa.gov and http://wind.nasa.gov, respectively).

Acknowledgments
The authors gratefully acknowledge support from NASA's SSERVI institute via the DREAM2 and LEADER teams (grant #NNX14AG16 A). Research by Anthony Rasca was supported by an appointment to the NASA Postdoctoral Program at NASA Goddard Space Flight Center, administered by Universities Space Research Association under contract with NASA. S. Fatemi acknowledges the support from the Swedish National Space Agency grant #179/18. The hybrid model computations were enabled by resources provided by the Swedish National Infrastructure for Computing (SNIC) at HPC2N through project no. 2020/5–101, and the results are publicly available online (https://data.mendeley.com/datasets/gf9cj4k-fnw/1). MHD simulation results have been provided by the Community Coordinated Modeling Center at Goddard Space Flight Center through their public Runs on Request system (http://ccmc.gsfc.nasa.gov; run number Anthony_Rasca_090619_1). The OpenGGCM Model was developed by J. Raeder and T. Fuller-Rowell at the Space Science Center, University of New Hampshire. The THEMIS-ARTEMIS mission is funded and operated under NASA Grant #NAS5-02099 and we specifically acknowledge J. P. McFadden for the use of ESA data and K.-H. Glassmeier, U. Auster, and W. Baumjohann for the use of FGM data provided under the lead of the Technical University of Braunschweig with financial support through the German Ministry for Economy and the German Center for Aviation and Space (DLR), contract #50 OC 0302.

References

Angelopoulos, V. (2010). The ARTEMIS mission. *Space Science Reviews*, *165*, 3–25. https://doi.org/10.1007/s11214-010-9687-2

Auster, H. U., Glassmeier, K. H., Magnes, W., Aydogar, O., Baumjohann, W., Constantinescu, D., et al. (2008). The THEMIS fluxgate magnetometer. *Space Science Reviews*, *141*, 235–264.

Birch, P. C., & Chapman, S. C. (2001). Particle-in-cell simulations of the lunar wake with high phase space resolution. *Geophysical Research Letters*, *28*, 219–222.

Colburn, D. S., Currie, R. G., Mihalov, J. D., & Sonett, C. P. (1967). Diamagnetic solar-wind cavity discovered behind Moon. *Science*, *158*, 1040–1042.

Crow, J. E., Auer, P. L., & Allen, J. E. (1975). The expansion of a plasma into a vacuum. *Journal of Plasma Physics*, *14*, 65–76. https://doi.org/10.1017/S0022377800025538

Cui, F., & Lei, L. (2008). 2D MHD simulation of the lunar wake. *Chinese Journal of Space Science*, *28*, 189–193.

Dhanya, M. B., Bhardwaj, A., Futaana, Y., Barabash, S., Alok, A., Wieser, M., et al. (2016). Characteristics of proton velocity distribution functions in the near-lunar wake from Chandrayaan-1/SWIM observations. *Icarus*, *271*, 120–130. https://doi.org/10.1016/j.icarus.2016.01.032

Farrell, W. M., Kaiser, M. L., Steinberg, J. T., & Bale, S. D. (1998). A simple simulation of a plasma void: Applications to Wind observations of the lunar wake. *Journal of Geophysical Research*, *103*, 23653–23660.

Farrell, W. M., Stubbs, T. J., Halekas, J. S., Killen, R. M., Delory, G. T., Collier, M. R., & Vondrak, R. R. (2010). Anticipated electrical environment within permanently shadowed lunar craters. *Journal of Geophysical Research*, *115*, E03004. https://doi.org/10.1029/2009JE003464

Farrell, W. M., Tribble, A. C., & Steinberg, J. T. (2002). Similarities in the plasma wake of the Moon and space shuttle. *Journal of Spacecraft and Rockets*, *39*, 749. https://doi.org/10.2514/2.3874

Fatemi, S., Holmström, M., & Futaana, Y. (2012). The effects of lunar surface plasma absorption and solar wind temperature anisotropies on the solar wind proton velocity space distributions in the low-altitude lunar plasma wake. *Journal of Geophysical Research*, *117*, A10105. https://doi.org/10.1029/2011JA017353

Fatemi, S., Holmström, M., Futaana, Y., Barabash, S., & Lue, C. (2013). The lunar wake current systems. *Geophysical Research Letters*, *40*, 17–21. https://doi.org/10.1029/2012GL054635

Fatemi, S., Holmström, M., Futaana, Y., Lue, C., Collier, M. R., Barabash, S., & Stenberg, G. (2014). Effects of protons reflected by lunar crustal magnetic fields on the global lunar plasma environment. *Journal of Geophysical Research: Space Physics*, *119*, 6095–6115. https://doi.org/10.1002/2014JA019900

Fatemi, S., Poirier, N., Holmström, M., Lindkvist, J., Wieser, M., & Barabash, S. (2018). A modeling approach to infer the solar wind dynamic pressure from magnetic field observations inside Mercury's magnetosphere. *Astronomy and Astrophysics*, *614*, A132. https://doi.org/10.1051/0004-6361/201832764

Fatemi, S., & Poppe, A. R. (2018). Solar wind plasma interaction with asteroid 16 Psyche: Implication for formation theories. *Geophysical Research Letters*, *45*, 39–48. https://doi.org/10.1002/2017GL073980

Fatemi, S., Poppe, A. R., & Barabash, S. (2020). Hybrid simulations of solar wind proton precipitation to the surface of Mercury. *Journal of Geophysical Research: Space Physics*, *125*, e2019JA027706. https://doi.org/10.1029/2019JA027706

Fatemi, S., Poppe, A. R., Delroy, G. T., & Farrell, W. M. (2017). AMITIS: A 3D GPU-based hybrid-PIC model for space and plasma physics. *Journal of Physics: Conference Series*, *837*, 12017. https://doi.org/10.1088/1742-6596/837/1/012017

Fuqua Haviland, H., Poppe, A. R., Fatemi, S., Delory, G. T., & de Pater, I. (2019). Time-dependent hybrid plasma simulations of lunar electromagnetic induction in the solar wind. *Geophysical Research Letters*, *46*, 4151–4160. https://doi.org/10.1029/2018GL080523

Garrick-Bethell, I., Poppe, A. R., & Fatemi, S. (2019). The lunar paleo-magnetosphere: Implications for the accumulation of polar volatile deposits. *Geophysical Research Letters*, *46*, 5778–5787. https://doi.org/10.1029/2019GL082548

Halekas, J. S., Bale, S. D., Mitchell, D. L., & Lin, R. P. (2005). Electrons and magnetic fields in the lunar plasma wake. *Journal of Geophysical Research*, *110*, A07222. https://doi.org/10.1029/2004JA010991

Halekas, J. S., Delory, G. T., Lin, R. P., Stubbs, T. J., & Farrell, W. M. (2008). Lunar Prospector observations of the electrostatic potential of the lunar surface and its response to incident currents. *Journal of Geophysical Research*, *113*, A09102. https://doi.org/10.1029/2008JA013194

Halekas, J. S., Delory, G. T., Lin, R. P., Stubbs, T. J., & Farrell, W. M. (2009). Lunar Prospector measurements of secondary electron emission from lunar regolith. *Planetary and Space Science*, *57*, 78–82. https://doi.org/10.1016/j.pss.2008.11.009

Halekas, J. S., Poppe, A. R., & McFadden, J. P. (2014). The effects of solar wind velocity distributions on the refilling of the lunar wake: ARTEMIS observations and comparisons to one-dimensional theory. *Journal of Geophysical Research: Space Physics*, *119*, 5133–5149. https://doi.org/10.1002/2014JA020083

Halekas, J. S., Saito, Y., Delory, G. T., & Farrell, W. M. (2011). New views of the lunar plasma environment. *Planetary and Space Science*, *59*, 1681–1694. https://doi.org/10.1016/j.pss.2010.08.011

Harada, Y., Machida, S., Halekas, J. S., Poppe, A. R., & McFadden, J. P. (2013). ARTEMIS observations of lunar dayside plasma in the terrestrial magnetotail lobe. *Journal of Geophysical Research: Space Physics*, *118*, 3042–3054. https://doi.org/10.1002/jgra.50296

Harada, Y., Poppe, A. R., Halekas, J. S., Chamberlin, P. C., & McFadden, J. P. (2017). Photoemission and electrostatic potentials on the dayside lunar surface in the terrestrial magnetotail lobes. *Geophysical Research Letters*, *44*, 5276–5282. https://doi.org/10.1002/2017GL073419

Harnett, E. M., & Winglee, R. M. (2013). Flux rope passage at the Moon while in the terrestrial magnetotail. *Advances in Space Research*, *52*, 243–250.

Holmström, M., Fatemi, S., Futaana, Y., & Nilsson, H. (2012). The interaction between the Moon and the solar wind. *Earth Planets and Space*, *64*, 237–245.

Jackman, C. M., Slavin, J. A., Kivelson, M. G., Southwood, D. J., Achilleos, N., Thomsen, M. F., et al. (2014). Saturn's dynamic magnetotail: A comprehensive magnetic field and plasma survey of plasmoids and traveling compression regions and their role in global magnetospheric dynamics. *Journal of Geophysical Research: Space Physics*, *119*, 5465–5494. https://doi.org/10.1002/2013JA019388

Kiehas, S. A., Angelopoulos, V., Runov, A., Moldwin, M. B., & Möstl, C. (2012). On the formation of tilted flux ropes in the Earth's magnetotail observed with ARTEMIS. *Journal of Geophysical Research*, *117*, A05231. https://doi.org/10.1029/2011JA017377

Liu, Y. D., Luhmann, J. G., Lugaz, N., Möstl, C., Davies, J. A., Bale, S. D., & Lin, R. P. (2013). On Sun-to-Earth propagation of coronal mass ejections. *The Astrophysical Journal*, *769*, 45. https://doi.org/10.1088/0004-637X/769/1/45

Lui, A. T. Y. (1987). Road map to magnetotail domains. In A. T. Y. Lui (Ed.), *Magnetotail physics*. Baltimore, MD: Johns Hopkins University Press.

Manka, R. H. (1973). Plasma and potential at the lunar surface. *Astrophysics and Space Science*, *37*, 347–361. https://doi.org/10.1007/978-94-010-2647-5_22

Ma, Y., Wong, H.-C., & Xu, X. (2015). Subsonic and sunward-orientated lunar wake observed by ARTEMIS in the geomagnetotail. *Astrophysics Space Science*, *358*, 34. https://doi.org/10.1007/s10509-015-2430-4

McFadden, J. P., Carlson, C. W., Larson, D., Ludlam, M., Abiad, R., Elliott, B., et al. (2008). The THEMIS ESA plasma instrument and in-flight calibration. *Space Science Reviews*, *141*, 277–302.

Nishino, M. N., Harada, Y., Saito, Y., Tsunakawa, H., Takahashi, F., Yokota, S., et al. (2017). Kaguya observations of the lunar wake in the terrestrial foreshock: Surface potential change by bow-shock reflected ions. *Icarus*, *293*, 45–51. https://doi.org/10.1016/j.icarus.2017.04.005

Nishino, M. N., Maezawa, K., Fujimoto, M., Saito, Y., Yokota, S., Asamura, K., et al. (2009). Pairwise energy gain-loss feature of solar wind protons in the near-Moon wake. *Geophysical Research Letters*, *36*, L12108. https://doi.org/10.1029/2009GL039049

Patsourakos, S., Georgoulis, M. K., Vourlidas, A., Nindos, A., Sarris, T., Anagnostopoulos, G., et al. (2016). The major geoeffective solar eruptions of 2012 March 7: Comprehensive Sun-to-Earth analysis. *The Astrophysical Journal*, *817*, 14. https://doi.org/10.3847/0004-637X/817/1/14

Poppe, A. R. (2019). Comment on "The dominant role of energetic ions in solar wind interaction With the Moon" by Omidi et al. *Journal of Geophysical Research: Space Physics*, *124*, 6927–6932. https://doi.org/10.1029/2019JA026692

Poppe, A. R., Fatemi, S., Halekas, J. S., Holmström, M., & Delory, G. T. (2014). ARTEMIS observations of extreme diamagnetic fields in the lunar wake. *Geophysical Research Letters*, *41*, 3766–3773. https://doi.org/10.1002/2014GL060280

Poppe, A., Halekas, J. S., & Horányi, M. (2011). Negative potentials above the day-side lunar surface in the terrestrial plasma sheet: Evidence of non-monotonic potentials. *Geophysical Research Letters*, *38*, L02103. https://doi.org/10.1029/2010GL046119

Poppe, A., & Horányi, M. (2010). Simulations of the photoelectron sheath and dust levitation on the lunar surface. *Journal of Geophysical Research*, *115*, A08106. https://doi.org/10.1029/2010JA015286

Raeder, J., Larson, D., Li, W., Kepko, E. L., & Fuller-Rowell, T. (2008). OpenGGCM simulations for the THEMIS mission. *Space Science Reviews*, *141*, 535–555. https://doi.org/10.1007/s11214-008-9421-5

Rhodes, E. M., & Farrell, W. M. (2019). Steady-state solution of a solar wind-generated electron cloud in a lunar crater. *Journal of Geophysical Research: Space Physics*, *124*, 4983–4993. https://doi.org/10.1029/2019JA026625

Richardson, I. G., & Cane, H. V. (2010). Near-Earth interplanetary coronal mass ejections during Solar Cycle 23 (1996-2009): Catalog and summary of properties. *Solar Physics*, *264*, 189–237. https://doi.org/10.1007/s11207-010-9568-6

Roux, A., Le Contel, O., Coillot, C., Bouabdellah, A., de la Porte, B., Alison, D., et al. (2008). The search coil magnetometer for THEMIS. *Space Science Reviews*, *141*, 265–275. https://doi.org/10.1007/s11214-008-9455-8

Shang, W. S., Tang, B. B., Shi, Q. Q., Tian, A. M., Zhou, X.-Y., Yao, Z. H., et al. (2020). Unusual location of the geotail magnetopause near lunar orbit: A case study. *Journal of Geophysical Research: Space Physics*, *125*, e2019JA027401. https://doi.org/10.1029/2019JA027401

Sibeck, D. G., & Lin, R.-Q. (2014). Size and shape of the distant magnetotail. *Journal of Geophysical Research: Space Physics*, *119*, 1028–1043. https://doi.org/10.1002/2013JA019471

Spreiter, J. R., Marsch, M. C., & Summers, A. L. (1970). Hydromagnetic aspects of solar wind flow past the Moon. *Cosmic Electrodynamics*, *1*, 5.

Troshichev, O., Kokubun, S., Kamide, Y., Nishida, A., Mukai, T., & Yamamoto, T. (1999). Convection in the distant magnetotail under extremely quiet and weakly disturbed conditions. *Journal of Geophysical Research*, *104*, 10249–10264. https://doi.org/10.1029/1998JA900141

Vernisse, Y., Kriegel, H., Wiehle, S., Motschmann, U., & Glassmeir, K. H. (2013). Stellar winds and planetary bodies simulations: Lunar type interaction in super-Alfvénic and sub-Alfvénic flows. *Planetary Space Science*, *84*, 37–47. https://doi.org/10.1016/j.pss.2013.04.004

Wang, Y.-C., Müller, J., Ip, W.-H., & Motschmann, U. (2011). A 3D hybrid simulation study of the electromagnetic field distributions in the lunar wake. *Icarus*, *216*, 415–425. https://doi.org/10.1016/j.icarus.2011.09.021

Xie, L. H., Li, L., Zhang, Y. T., & De Zeeuw, D. L. (2013). Three-dimensional MHD simulation of the lunar wake. *Science China Earth Sciences*, *56*, 330–338. https://doi.org/10.1007/s11430-012-4383-6

Xu, S., Poppe, A. R., Halekas, J. S., Mitchell, D. L., McFadden, J. P., & Harada, Y. (2019). Mapping the lunar wake potential structure with ARTEMIS data. *Journal of Geophysical Research: Space Physics*, *119*, 3360–3377. https://doi.org/10.1029/2019JA026536

Zhang, H., Khurana, K. K., Kivelson, M. G., Angelopoulos, V., Wan, W. X., Liu, L. B., et al. (2014). Three-dimensional lunar wake reconstructed from ARTEMIS data. *Journal of Geophysical Research: Space Physics*, *119*, 5220–5243. https://doi.org/10.1002/2014JA020111

Zimmerman, M. I., Farrell, W. M., Stubbs, T. J., Halekas, J. S., & Jackson, T. L. (2011). Solar wind access to lunar polar craters: Feedback between surface charging and plasma expansion. *Geophysical Research Letters*, *38*, L19202. https://doi.org/10.1029/2011GL048880